ELSEVIER

Inorganica Chimica Acta 275–276 (1998) 192–202

Inorganica Chimica Acta

Gas-phase positive and negative ion chemistry of methyl hydroperoxide

Massimiliano Aschi [a], Marina Attinà [b,*], Fulvio Cacace [a], Romano Cipollini [a], Federico Pepi [a]

[a] *Università 'La Sapienza', P.le A. Moro 5, 00185 Rome, Italy*

[b] *Università 'Tor Vergata', Via della Ricerca Scientifica, 00133 Rome, Italy*

Received 5 June 1997; revised 14 August 1997; accepted 26 September 1997

Abstract

The gas-phase ion chemistry of methyl hydroperoxide (**1**) was investigated by mass spectrometric and theoretical methods. The proton affinity of **1**, 173.3 ± 2 kcal mol^{-1} measured by the FT-ICR bracketing technique and the kinetic method, is in excellent agreement with the value of 172.6 ± 2 kcal mol^{-1} from G2 ab initio calculations, which identify the α oxygen atom as the most basic site. Methylation of **1** by $(CH_3)_2F^+$ gives a mixed population of ions methylated at both oxygen atoms. The experimental proton affinity of CH_3OOCH_3 is 176.2 ± 4 kcal mol^{-1}, versus a theoretically computed value of 180.4 ± 2 kcal mol^{-1}, the most nucleophilic site being again the α oxygen atom. Nitrosation of **1** yields a $(CH_3OOH \cdot NO)^+$ adduct that behaves as both a nitrosating and a protonating agent. The results are discussed and compared with earlier pertinent studies.

Keywords: Gas-phase chemistry; Organic hydroperoxides

1. Introduction

The gas-phase chemistry of organic peroxides is currently the focus of active interest, owing to the growing recognition of their role in a variety of processes relevant to atmospheric pollution and combustion phenomena [1–8]. Although most of the studies concern neutral peroxides and derived reactive species, considerable attention has been devoted to the radical cations $M^{\cdot+}$ and their unimolecular fragmentation [9–14], whereas relatively few studies have been reported on the $[M+E]^+$ ions formed by the addition to organic peroxides of gaseous cations such as H^+, Cr^+, Co^+, and other simple ions [15–17]. As a continuation of our sustained research effort in the field of gas-phase ion chemistry [18], we report here the results of a joint experimental and theoretical study of the positive and negative gas phase ion chemistry of CH_3OOH (**1**), the most simple organic hydroperoxide, aimed in particular at evaluating its proton affinity (PA) and gas-phase acidity (GPA), as well as the structure and the relative stability of typical $(\mathbf{1}+E)^+$ adducts, where $E^+ = H^+$, CH_3^+ and NO^+.

* Corresponding author. Tel.: +39 6 7259 4337; fax: +39 6 7259 4328; e-mail: attina@stc.uniroma2.it

0020-1693/98/$19.00
PII S0020-1693(97)06077-5

2. Experimental

2.1. Materials

The gases were obtained from Matheson Gas Products or Aldrich Chemicals with a stated purity exceeding 99.95 mol%. Most of the other chemicals were research grade products from commercial sources. The reaction of $(CH_3)_2SO_4$ (or $(CD_3)_2SO_4$) with H_2O_2 in a basic solution was utilized to prepare CH_3OOH (or CD_3OOH), which were analysed by positive and negative CH_4/chemical ionization (CI) mass spectrometry, utilizing a VG Micromass Trio 1 benchtop instrument.

2.2. FT-ICR experiments

A model 47e Apex FT-ICR mass spectrometer from Bruker Spectrospin AG, equipped with an 'infinity' cell and an external EI/CI ion source was used. In the 'bracketing' experiments $(CH_3OOH)H^+$ ions, generated in the external source by CH_4/CI (10^{-5} Torr) were driven into the resonance cell, isolated by broad-band and single 'shot' ejection, allowed to cool by a 2 s delay before undergoing reaction with the neutral, contained in the cell at pressures from 10^{-8} to 10^{-7} Torr. The equilibrium method applied to evaluation of the PA of CH_3OOCH_3 involved formation of $(CH_3OOCH_3)H^+$ ions

by CH_4/CI in the external source, their isolation and reaction with CH_3OOCH_3/CF_3COCH_3 mixtures of known composition obtained from the vaporization of premixed liquid mixtures, each experiment being performed in triplicate in order to evaluate the reproducibility of the results. The pressure readings of the ionization gauge were corrected according to established procedures [19].

2.3. TQ experiments

The low-energy CAD experiments were performed in a model Quattro VG Micromass triple quadrupole spectrometer. The parent ions were generated in the CH_4/CI source (0.1 Torr, repeller voltage 0 V), selected with the first quadrupole and allowed to collide with Ar in the RF-only hexapolar cell at target thicknesses not exceeding 9×10^{12} cm^2 in order to minimize multiple collisions with an axial kinetic energy from 10 to 120 eV (laboratory framework). The charged fragments formed were analysed with the third quadrupole operated in the scan mode (150 amu s^{-1}).

2.4. MIKE and CAD spectra

The spectra were recorded using a ZAB-2F reverse geometry mass spectrometer from VG Micromass, equipped with an EI/CI ion source. The protonated ions were generated by CH_4/CI ($\sim$0.2 Torr), typical experimental conditions being as follows: source temperature, 150°C; electron current, 1 mA; electron energy, 50 V; repeller voltage, 0 V; mass resolving power, 2×10^3; energy resolution, 4×10^3. The CAD spectra were taken by admitting He into the collision cell up to a pressure ensuring a 30% reduction of the main beam intensity, each spectrum being the average of 50 scans.

3. Experimental results

3.1. Evaluation of the proton affinity of CH_3OOH

Protonation of **1** is readily accomplished under chemical ionization (CI) conditions utilizing the reaction

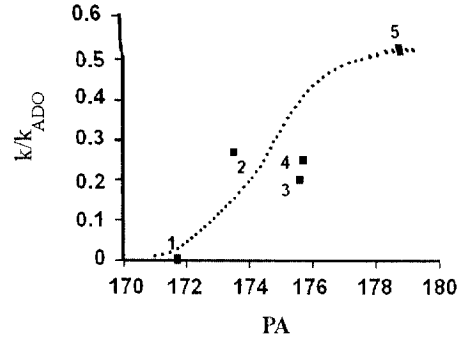

Fig. 1. Collisional efficiency of the proton transfer (2) from $(CH_3OOH)H^+$ to selected bases: (1) CH_2O, (2) CH_3COCF_3, (3) $CH_2(CN)_2$, (4) o-$C_6H_4F_2$, (5) HCOOH.

$$\mathbf{1}+AH^+ \rightarrow (CH_3OOH)H^+ + A \qquad (1)$$

where A = CH_4, C_2H_4, C_3H_6, and H_2O. Evaluation of the PA of **1** by the ICR equilibrium method is prevented by the decomposition of methyl hydroperoxide, a process which is known [20] to occur on metal surfaces, e.g. on the leak valves of the FT-ICR spectrometer, not readily replaceable by inert materials. The alternative 'bracketing' technique [21], based on the rate of proton transfer from $(CH_3OOH)H^+$ to selected bases, was adopted. To this end, the ion, formed via Eq. (1) in the external CI source of the FT-ICR spectrometer, was isolated by selective-ejection techniques and allowed to react with a gaseous base B in the resonance cell, according to the process

$$(CH_3OOH)H^+ + B \rightarrow \mathbf{1} + BH^+ \qquad (2)$$

which can be accompanied by other reactions, such as charge exchange and methyl transfer, depending on the specific base employed (Table 1). Actually, these experiments, like the others aimed at evaluating the PA of **1**, were performed utilizing CD_3OOH to make sure that the ion assayed had undergone no rearrangements. The efficiency of Eq. (2), evaluated from the ratio between the rate constant and the collision rate constant calculated in turn according to the ADO theory [23], is illustrated in Fig. 1 and leads to an estimated PA for **1** of 174 ± 2 kcal mol^{-1}. An independent set of experiments,

Table 1
Rate constants and collisional efficiencies for the deprotonation of $(CH_3OOH)H^+$ ions by bases of different strength

Base	PA (kcal mol^{-1})	Rate constant $\times10^{-10}$ (cm^3 s^{-1} molecule^{-1}) [a] (efficiency)		
		H^+ transfer	CH_3^+ transfer	Charge exchange
HCOOH	178.8 [b]	7.2 (0.52)	2.9 (0.21)	
o-$C_6H_4F_2$	175.7 [c]	6.0 (0.30)	1.0 (0.05)	2.6 (0.13)
$H_2C(CN)_2$	175.6 [b]	5.0 (0.20)		
CH_3COCF_3	173.5 [c]	4.3 (0.24)	0.52 (0.03)	
1,2,3-$C_6H_3F_3$	173.0 [c]	5.1 (0.23)	0.26 (0.01)	1.6 (0.07)
HCHO	171.7 [b]	0.052 (0.002)		

[a] Estimated uncertainty of rate constants, $\pm$30%. Efficiencies evaluated from the collision rate constants, calculated from the ADO theory, see text.
[b] From Ref. [21].
[c] From Ref. [22].

based on the kinetic method [24], involved the measurement of the branching ratio

$$(CH_3OOH\cdot H^+\cdot B) \longrightarrow (CH_3OOH)H^+ + B \quad (3a)$$

$$(CH_3OOH\cdot H^+\cdot B) \longrightarrow CH_3OOH + BH^+ \quad (3b)$$

in the metastable fragmentation of the proton-bound dimers formed by **1** with suitable gaseous bases. Eq. (3a) predominates when $B = CH_2O$, PA = 171.7 kcal mol^{-1}, whereas Eq. (3b) predominates when $B = CF_3COCH_3$, PA = 173.5 kcal mol^{-1} [23], leading to $PA(CH_3OOH) = 172.6 \pm 2$ kcal mol^{-1}. Combination of the results from the ICR bracketing technique with those from the kinetic method leads to an experimental estimate of $PA(CH_3OOH) = 173.3 \pm 2$ kcal mol^{-1}.

3.2. MIKE and CAD spectra of $(CH_3OOH)H^+$ ions

Either of the oxygen atoms of **1** can undergo protonation, yielding protomers that can subsequently isomerize into the more stable (vide infra) proton-bound dimer **PBD**

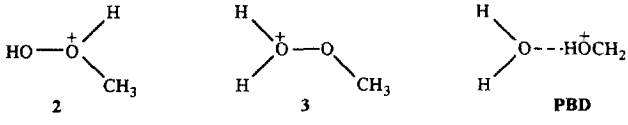

2 **3** **PBD**

It is likely that exothermic protonation of **1** can produce mixed ionic populations, whose structural analysis was attempted by comparing their MIKE and CAD spectra with those of model **PBD** obtained from the H_2O/CI of CH_2O. The MIKE spectra display significant differences, in that the $(CH_3OOH)H^+$ ions from Eq. (1), $A = H_2O$, give two charged fragments, the major one of $m/z = 31$, accompanied by a fragment of $m/z = 19$. Assignment of the fragments was facilitated by recording the MIKE spectra of $(CD_3OOH)H^+$ ions, characterized by a CD_2HO^+ fragment, $m/z = 33$ (21%), a CD_3O^+ fragment, $m/z = 34$ (72%), and an H_2DO^+ fragment, $m/z = 20$ (7%). By contrast, the only significant charged fragment in the MIKE spectra of model **PBD** is CH_3O^+, $m/z = 31$, most likely protonated formaldehyde. The high-energy (8 keV) CAD spectra of the $(CX_3OOH)H^+$ ions (X = H, D) from the protonation of **1** by H_3O^+ are compared in Table 2 with that of the model **PBD**. Based on the mass shifts observed in passing from X = H to X = D, the most abundant fragments from $(CH_3OOH)H^+$ ions produced by proton transfer (Eq. (1)) are CH_3^+ (10%), CHO^+ (27%), CH_4O^+ (19%) and $CH_4O_2^+$ (17%). By contrast, the CAD spectrum of **PBD** displays no CH_3^+, CH_4O^+ and $CH_4O_2^+$ ions, the most abundant fragments being H_3O^+ (50%) and CHO^+ (28%). Using the TQ spectrometer, low-energy CAD spectra were recorded, also showing significant differences between $(CH_3OOH)H^+$ ions from Eq. (1) and the model **PBD**, which remarkably gives almost exclusively (92%) the CH_3O^+ fragment. In summary, the CAD and MIKE results do not allow positive discrimination between protomers **2** and **3**, a situation which occurs frequently when the connectivity of the species examined differs exclusively as to the location of a single proton. However, the results speak against complete conversion of **2** and/or **3** into **PBD** in the time scale (~10 ms) of MIKE and CAD spectrometry.

3.3. Methylation of CH_3OOH

The alkylation, performed by CH_3F/CI according to the process

$$(CH_3)_2F^+ + \mathbf{1} \rightarrow CH_3F + (CH_3OOH)CH_3^+ \quad (4)$$

can occur at either oxygen atom, giving the isomeric oxonium ions

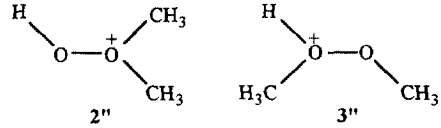

2″ **3″**

Model **3″** ions were prepared by CH_4/CI of CH_3OOCH_3 according to the process

$$C_nH_5^+ (n = 1,2) + CH_3OOCH_3 \rightarrow C_nH_4 + \mathbf{3''} \quad (5)$$

The MIKE and CAD spectra of the ionic populations from Eqs. (4) and (5) are compared in Tables 3 and 4. The salient feature of the MIKE spectra of the $(CH_3OOH)CH_3^+$ ions from Eq. (4) is the presence of peaks at $m/z = 45$ and 46 (shifted to 47, 48 and 49 in the spectra of $(CD_3OOH)CH_3^+$). These fragments, identified as $H_3C–O–CH_2^+$ and $H_3C–O–$

Table 2
CAD spectra of $(CX_3OOH)H^+$ (X = H,D) and $(CH_2O^+H\cdots OH_2)^+$ ions

Ion	Formation process	Relative intensity of fragments at values of m/z (%) [a]													
		15	18	19	29	30	31	32	33	34	35	47	48	49	51
$(CH_3OOH)H^+$	$CH_3OOH + H_3O^+$	10		[b]	27	8	[b]	18		5		9	17		
$(CH_3OOH)H^+$ [c]	$CH_3OOH + H_3O^+$				15		57	28							
$(CD_3OOH)H^+$	$CD_3OOH + H_3O^+$		14			25		10	[b]	[b]	18			13	15
$(CH_2OH^+\cdots OH_2)$	$CH_2O + H_3O^+$		6	50	28	11	[b]								
$(CH_2OH^+\cdots OH_2)$ [c]	$CH_2O + H_3O^+$ [c]			5			92								

[a] Intensities are normalized to the sum of the intensities of all CAD fragments. Fragments whose intensities are below 5% are omitted. Estimated errors ±10%.
[b] These fragments are present in the MIKE spectra and therefore are omitted.
[c] Low-energy CAD spectra, see text.

Table 3
MIKE spectra of $C_2X_3H_4O_2^+$ ions from the methylation of CX_3OOH by $(CH_3)_2F^+$ and the protonation of CH_3OOCH_3 by $C_nH_5^+$ ($n=1,2$)

Ion	Source	Relative intensity of fragments at values of m/z (%) [a]							
		31	33	34	45	46	47	48	49
$(CH_3OOH)CH_3^+$	Methylation	7	34		45	14			
$(CD_3OOH)CH_3^+$	Methylation			18			17	42	23
$(CH_3OOCH_3)H^+$	Protonation	19	81						

[a] Standard deviation of relative intensities ±20%.

Table 4
CAD spectra of $C_2H_7O_2^+$ ions from the methylation of CH_3OOH by $(CH_3)_2F^+$, population A, and the protonation of CH_3OOCH_3 by $C_nH_5^+$ ($n=1,2$), population B

m/z	Population A	Population B
15	12	21
29	12	30
30	3	20
32	4	17
45	35	3
46	29	2
47	3	4
48	2	3

Ions arising from metastable fragmentation are not taken into account. Standard deviation of relative intensity ±20%.

CH_3^+ ions, are suggestive of the C–O–C connectivity typical of **2″** and are not detectable in the MIKE spectra of model **3″** ions from Eq. (5). The same situation characterizes the CAD spectra where, at variance with model ions **3″** from Eq. (5), the $(CH_3OOH)CH_3^+$ ions from Eq. (4) give abundant fragments of $m/z=45$ and 46, again suggestive of the C–O–C connectivity typical of **2″**. In summary, the MIKE and CAD results show that at least a fraction of the $(CH_3OOH)CH_3^+$ ions from Eq. (4) has the **2″** structure.

3.4. Evaluation of the proton affinity of CH_3OOCH_3

The ICR equilibrium method was used, for the reaction

$$(CH_3OOCH_3)H^+ + CH_3COCF_3 \rightleftharpoons CH_3OOCH_3 + (CH_3COCF_3)H^+ \quad (6)$$

promoted by $(CH_3OOCH_3)H^+$ ions, produced in the external CI source of the spectrometer. The rapid prototropic equilibrium is disturbed at long reaction times by the incursion of the slower CH_3^+-transfer reaction to CH_3COCF_3, whose interference can be minimized by approaching equilibrium Eq. (6) from the other side. The ΔG_6° was estimated to be 2.7 kcal mol^{-1} at 298 K which, under the customary assumption [21] $\Delta G_6^\circ \cong \Delta H_6^\circ$ and utilizing the known PA of CH_3COCF_3, 173.5 kcal mol^{-1} [22], leads to a PA for CH_3OOCH_3 of 176.2 ± 4 kcal mol^{-1}. The unusually large error bar reflects the problems arising from the relatively large difference in ΔPA between the bases utilized, and from the incursion of the CH_3^+-transfer reaction.

3.5. Nitrosation of CH_3OOH

The addition process

$$NO^+ + \mathbf{1} \rightarrow (CH_3OOH)NO^+ \quad (7)$$

readily occurs in CH_3ONO/CI of methyl hydroperoxide. The MIKE spectrum of the nitrosated adduct shows only dissociation into the monomers, suggestive of their electrostatic, or loosely covalent, association. It should be noted that the lack of the CH_2ONO^+ fragment of $m/z=60$ tends to exclude isomerization of the initial product from Eq. (7) into the NO^+ bound (H_2CO–(NO^+)–OH_2) complex. The binding energy (BE) of NO^+ to **1** was estimated by the kinetic method [21] based on the metastable fragmentation of $(CH_3OOH)NO^+L$ nitrosonium-bound dimers where L denotes a suitable ligand, e.g. i-C_3H_7Cl, whose NO^+ BE amounts to 21.4 kcal mol^{-1} [25]. From the experimentally measured $[CH_3OOH \cdot NO^+]/[i\text{-}C_3H_7Cl \cdot NO^+]$ intensity ratio, and utilizing the appropriate calibration factor derived from a comprehensive study of NO^+ BEs [25], a value of 22.4 ± 3 kcal mol^{-1} for the NO^+ BE of **1** was estimated.

Table 5
Reactivity of $(CH_3OOH)NO^+$ ions toward selected nucleophiles

Nucleophile	k (10^9 cm^3 s^{-1} molecule^{-1}) [a]	k_{ADO} (10^9 cm^3 s^{-1} molecule^{-1}) [b]	Efficiency (%)	Relative efficiency (%)
CH_3OH	0.48	1.5	32	nitrosation 16, protonation 84
NH_3	0.50	1.7	30	nitrosation 40, protonation 60
C_6H_6	0.54	1.2	46	nitrosation 37, protonation 7, charge exchange 56

[a] Estimated uncertainty of the experimental rate constant ±20%. The data refer to the overall reactivity toward the nucleophile.
[b] Calculated according to Ref. [23].

The adduct from Eq. (7) was further examined by FT-ICR mass spectrometry, investigating its reactivity toward selected nucleophiles, Nu. The results, summarized in Table 5, demonstrate the operation of two general processes

$$(CH_3OOH)NO^+ + Nu \rightarrow NuNO^+ (+ CH_3OOH) \quad (8a)$$

$$(CH_3OOH)NO^+ + Nu \rightarrow NuH^+ (+ CH_3OONO) \quad (8b)$$

This observation is of interest, suggesting either the presence of a single adduct capable of behaving both as a nitrosating and a protonating agent, or the presence of two distinct adducts, characterized by nitrosating and protonating properties respectively.

3.6. Evaluation of the gas-phase acidity of CH_3OOH

The CH_3OO^- anion, readily formed in the negative CH_4/CI of **1**, undergoes no metastable decomposition, giving only a minor O_2^- fragment in CAD experiments. The GPA of **1** was evaluated by the kinetic method, measuring the relative intensity of the CH_3OO^- and L^- fragments from the metastable decomposition of $(CH_3OO \cdot H \cdot L)^-$ proton-bound dimers, where HL denotes a neutral ligand of known GPA [21]. The 'effective' temperature of the proton-bound dimers was obtained from a calibration plot constructed utilizing *n*- and t-butanol, *n*-hexanol, 3-methyl-3-pentanol and benzyl alcohol, whose GPA values are reported in the literature [21]. An effective temperature of 364 K was obtained from the satisfactorily linear calibration plot (correlation coefficient 0.998), and used to derive the GPA of CH_3OOH, 365.1 ± 4 kcal mol^{-1}.

4. Computational results

The structure, stability and isomerization pathway of the species of interest were investigated by ab initio methods. The level of theory, and the basis set were chosen according to the complexity of the specific system investigated, as described in detail below. All calculations were performed utilizing an IBM RISC/6000 version of the Gaussian 94 suite of programs [26].

4.1. Protonation of CH_3OOH

The geometries of the species of interest, optimized in the full space of the coordinates by analytical, gradient-based techniques in the framework of the second-order Møller–Plesset (MP2) perturbation theory, utilizing the 6-31G(d) basis set, are illustrated in Fig. 2. The zero-point vibrational energy corrections were computed at the same MP2(full)/6-31G(d) level of theory, also employed in the calculation of the harmonic vibrational frequencies of all stationary points identified in order to characterize them as true minima, transition states (TS) or higher-order saddle points. In addition, the STQN method [27] was applied for the search of all the maxima. The absolute G2 energies (0 K) are reported in Table 6, together with the absolute 298 K energies and utilized to construct the potential energy diagram of Fig. 3. The theoretically estimated PA(CH_3OOH) relative to formation of the most stable protomer **2** is 172.6 ± 2 kcal mol^{-1}, in excellent agreement with the experimental value of 173.3 ± 2 kcal mol^{-1}. At this level of theory, the PA of the terminal oxygen atom of **1** amounts to 168.1 ± 2 kcal mol^{-1}, reflecting the lower stability of **3** than of **2**. At the G2 level of theory, a large barrier, ~37 kcal mol^{-1}, is calculated for the conversion of **2** into **3**, whereas isomerization of **3** into the more stable [1] **PBD 5** is energetically less unfavourable.

[1] From Ref. [21], the combined heats of formation of CH_2OH^+ and H_2O amount to 110.2 kcal mol^{-1}. This sets an upper limit to the $\Delta DH_f°$ of the $(CH_2OH \cdots H_2O)$ **PBD**. In the same way, the combined heats of formation of CH_3CHOH^+ and H_2O amount to 81.2 kcal mol^{-1}, and those of CH_3OH^+ and CH_2O to 110 kcal mol^{-1}. These values represent the upper limits of the heats of formation of the $(CH_3CHOH\text{–}H_2O)$ and $(CH_3OH_2\text{–}OCH_2)$ **PBD** respectively.

Table 6
G2 absolute energies (hartree $molecule^{-1}$) at 0 and 298 K

Species		N [a]	E (0 K)	E (298 K)
1	CH_3OOH (C_1)	0	−190.58237	−190.57804
2	CH_3OHOH^+ (C_1)	0	−190.85611	−190.85166
3	$CH_3OOH_2^+$ (C_s)	0	−190.84898	−190.84449
4	TS **2/3** (C_1)	1 (i 2372.0 cm^{-1})	−190.79684	−190.79243
5	$CH_2O\text{–}H\text{–}OH_2^+$ (C_1)	0	−190.98449	−190.97886
6	$H_2O\text{–}CH_2OH^+$ (C_1)	0	−190.97283	−190.97721
7	TS **3/6** (C_s)	1 (i 934.7 cm^{-1})	−190.83161	−190.82683
8	TS **6/5** (C_1)	1 (i 248.2 cm^{-1})	−190.96372	−190.95849
9	CH_2OH^+ (C_s)	0	−114.60775	−114.60481
10	CH_2O (C_{2v})	0	−114.33891	−114.33604
11	H_2O (C_{2v})	0	−76.33205	−76.32921
12	H_3O^+ (C_s)	0	−76.59194	−76.58903
13	CH_3^+ (D_{3h})	0	−39.38559	−39.38273
14	H_2O_2 (C_2)	0	−151.36578	−151.36254
15	CH_3OO^- (C_s)	0	−189.99172	−189.98794

[a] Number of imaginary frequencies given in parentheses.

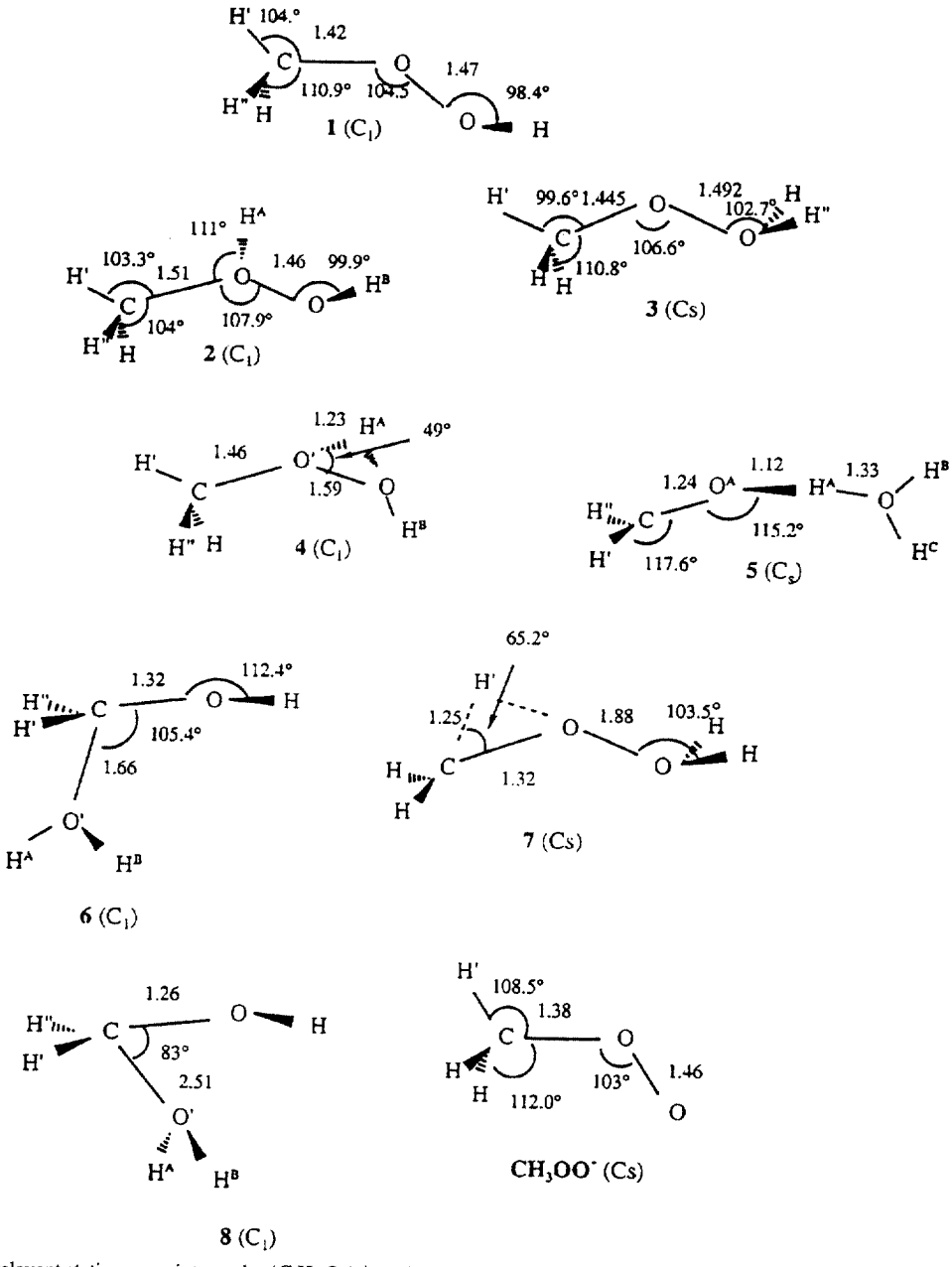

Fig. 2. Geometries of relevant stationary points on the $(C,H_5,O_2)^+$ surface and of the CH_3OO^- anion, optimized at the MP2(full)/6-31G(d) level of theory. Distances (Å), angles (°).

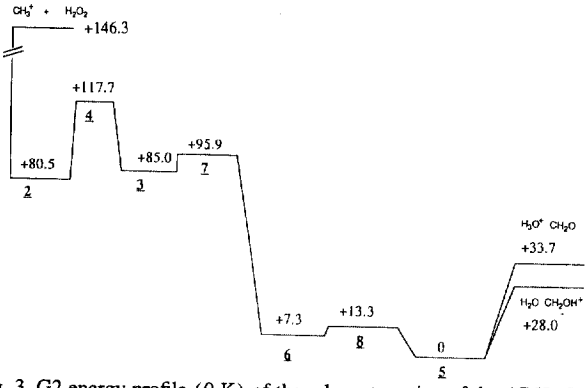

Fig. 3. G2 energy profile (0 K) of the relevant portion of the $(C,H_5,O_2)^+$ surface, see text. Energies in kcal mol^{-1}.

In fact, TS **7** is located only 10.9 kcal mol^{-1} over **3**, and the ensuing pathway from the minimum **6** to **5** is energetically downhill (Fig. 3).

Based on the G2 atomization energy of **1**, 530.5 kcal mol^{-1}, $\Delta H_f°(\mathbf{1})$ amounts to -31.6 ± 2 kcal mol^{-1}, consistent with previous results [28]. In view of the large endothermicity of the dissociation process

$$\mathbf{2} \rightarrow CH_3OH^{\cdot+} + OH \qquad (9)$$

computed to be 50.3 kcal mol^{-1} (298 K) at the G2 level of theory, **2** appears to be located in a sufficiently deep well to allow its experimental detection.

4.2. Methylation of CH_3OOH

Calculations up to the MP2(full)/6-31G(d) level of theory were performed to optimize the structures of relevant species (Fig. 4) and to evaluate the corresponding 0 K absolute energies, whereas the search and characterization of the saddle points were addressed at the G2 MP2 level of theory (Table 7). As apparent from the 0 K MP2(full)/6-31G(d) potential energy diagram illustrated in Fig. 5, structures **2″** and **3″** are in relatively deep wells, and their interconversion occurs via the TS **4″**, located ~45 kcal mol^{-1} above **2″**. Isomerization of **3″** into the much more stable [21] proton-bound dimers (**PBD″**), (CH_3CHOH^+–H_2O) and (CH_2-OH^+–$O(H)CH_3$), via TS **5″**, requires overcoming a 24.5 kcal mol^{-1} barrier, and hence is energetically favoured over **3″** → **2″** conversion. From Fig. 5, back dissociation of **3″** into **1** and CH_3^+ is endothermic by ~76 kcal mol^{-1}, and the endothermicity of dissociation into $(CH_3)_2O^+$ and OH can be calculated to be ~43 kcal mol^{-1} [21]. As a whole, the results characterize both **2″** and **3″** as sufficiently stable to be experimentally detectable. From the PA of CH_3OOCH_3, computed at the G2 MP2 level of theory to be 180.4 ± 2 kcal mol^{-1} at 298 K, and the atomization energy of CH_3OOCH_3, 804.4 kcal mol^{-1} at 298 K according to calculations per-

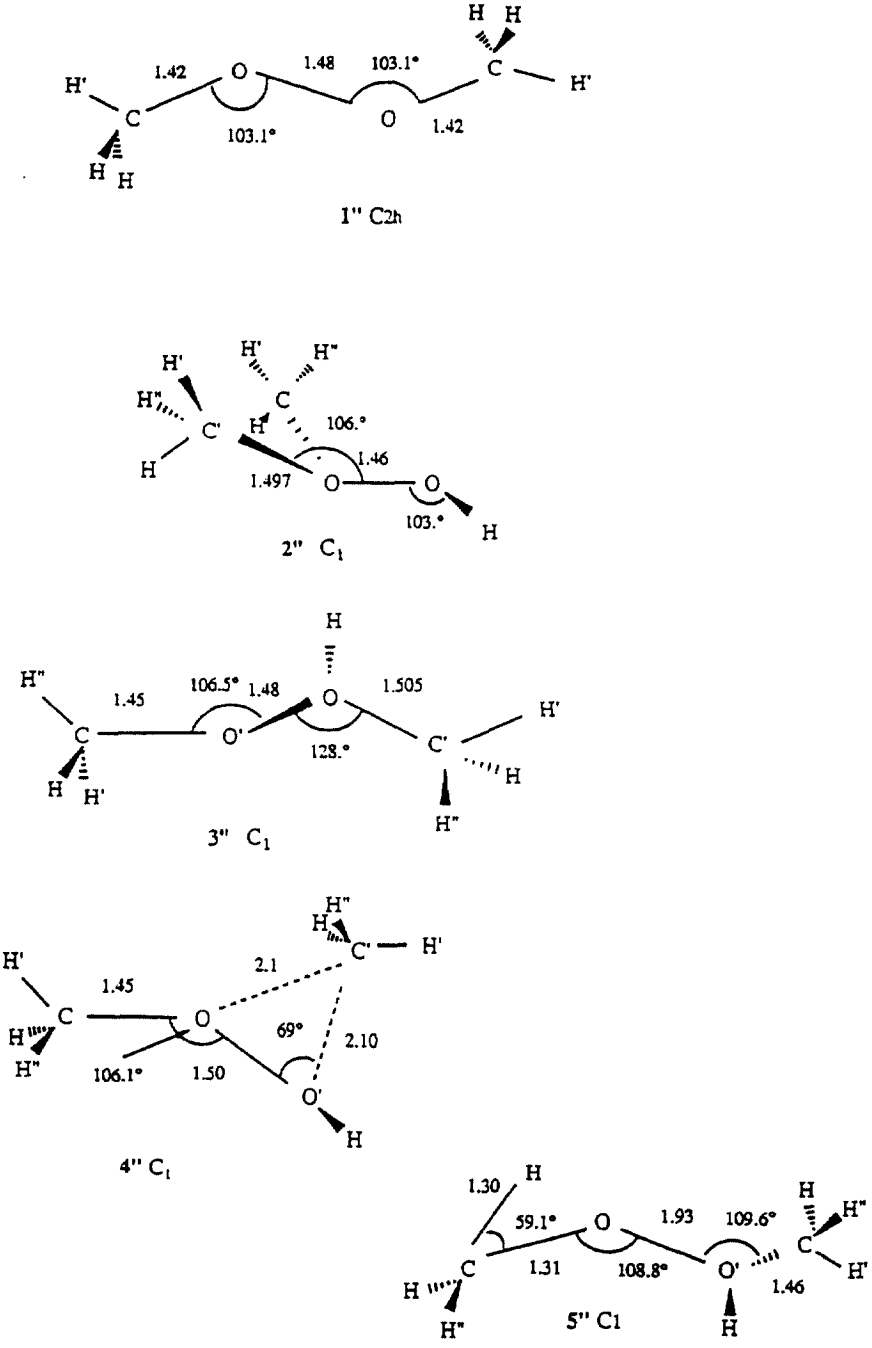

Fig. 4. Geometries of relevant stationary points on the $(C_2H_7O_2)^+$ surface optimized at the MP2(full)/6/31G(d) level of theory. Distances (Å), angles (°).

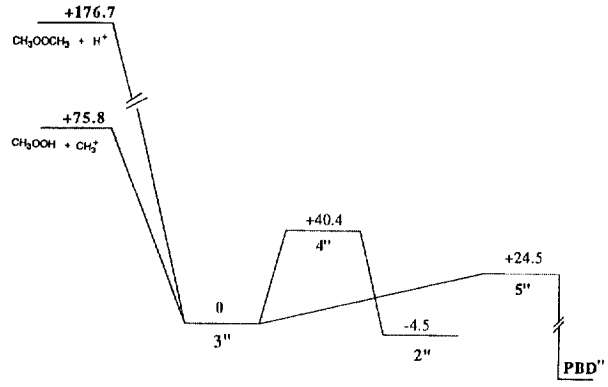

Fig. 5. G2 energy profile (0 K) of the relevant portion of the $(C_2,H_7,O_2)^+$ energy surface. Energies in kcal mol^{-1}.

formed at the same level of theory, the heats of formation of CH_3OOCH_3 and $(CH_3OOCH_3)H^+$ are estimated to be -32 ± 2 and 152.6 ± 4 kcal mol^{-1} respectively.

4.3. Nitrosation of CH_3OOH

The geometries were optimized at the MP2(full)/6-31G(d) level of theory, also employed to evaluate the ZPE and the thermal corrections to 298 K, whereas single point calculations were performed up to the MP4(STDQ)/6-311(d,p)//MP2(full)/6-31G(d) level of theory, the STQN method being applied to the search and characterization of the maxima [27]. The optimized geometries are illustrated in Fig. 6, the absolute energies at 0 and 298 K are reported in Table 8, and the potential energy diagram of the relevant species (0 K) is shown in Fig. 7.

Two isomeric $CH_3OOH \cdot NO^+$ complexes were found, characterized by a monomer separation larger than 2 Å, whose interconversion requires overcoming a small barrier (1.7 kcal mol^{-1}), well below the target accuracy of the computational approach. Hence, at the level of theory employed in the present study, **2′** → **1′** interconversion is to be regarded as a barrierless process. The global minimum is represented by **4′**, an adduct liable to dissociation into $CH_2ONO^+ + H_2O$ and/or into $CH_2O + H_2ONO^+$. It should be noted that a different entry into the $[C,H_4,N,O_3]^+$ hypersurface is represented by the protonation of methyl peroxonitrite, H_3COONO. The process was therefore investigated at the same level of theory, obtaining a PA for H_3COONO of 199.7 ± 4 kcal mol^{-1}, referred to the formation of **4′**, identified as the most stable isomer.

4.4. Gas-phase acidity of CH_3OOH

The geometry of the CH_3OO^- anion, optimized at the MP2(full)/6-31G(d) level of theory and reported in Fig. 2, is consistent with the results of previous calculations at the HF/6-31 + + G level of theory [29]. From the G2 absolute

Table 7
MP2(full)/6-31G(d) 0 K and 298 K absolute energies and G2 MP2 298 K absolute enthalpies (hartree $molecule^{-1}$)

Species		N^a	E (0 K)	E (298 K)	E (G2MP2)
1″	CH_3OOCH_3 (C_{2h})	0	−229.38015	−229.37460	−229.78738
2″	$CH_3OCH_3OH^+$ (C_1)	0	−229.66892	−229.66340	
3″	$CH_3OHOCH_3^+$ (C_s)	0	−229.66172	−229.65610	−230.07243
4″	TS **3″/2″** (C_1)	1 (i 713.9 cm^{-1})	−229.59725	−229.59134	
5″	TS **3″/PBD** (C_1)	1 (i 953.4 cm^{-1})		−229.62260	−229.61659

[a] Number of imaginary frequencies given in parentheses.

Table 8
MP4(SDTQ)/6-31G(d,p)//MP2(full)/6-31G(d)G2 0 and 298 K absolute energies (hartree $molecule^{-1}$)

Species		N^a	E (0 K)	E (298 K)
1″	$(CH_3OOH)NO^+$ (C_1)	0	−319.76647	−319.75984
2″	$(CH_3OOH)NO^+$ (C_1)	0	−319.76792	−319.76147
3″	TS 1″/2″ (C_1)	1 (i 132.7 cm^{-1})	−319.76372	−319.7573
4″	CH_2O–H_2ONO^+ (C_1)	0	−319.87232	−319.86381
5″	CH_3OHONO^+ (C_1)	0	−319.73933	−319.73313
6″	CH_3OONOH^+ (C_s)	0	−319.71207	−319.70662
7″	CH_3OONO (C_1)	0	−319.45117	−319.44556
8″	$(HONO)H^+$ (C_s)	0	−205.61096	−205.60570
9″	CH_2 (C_{2v})	0	−114.23534	−114.23248
10″	CH_3OOH (C_1)	0	−114.33891	−190.39738
11″	NO^+ ($C\infty_v$)	0	−129.32158	−129.31992
12″	CH_2–ONO^+ (C_s)	0	−243.59347	−243.58817
13″	H_2O (C_{2v})	0	−76.20966	−76.20683

[a] Number of imaginary frequencies given in parentheses.

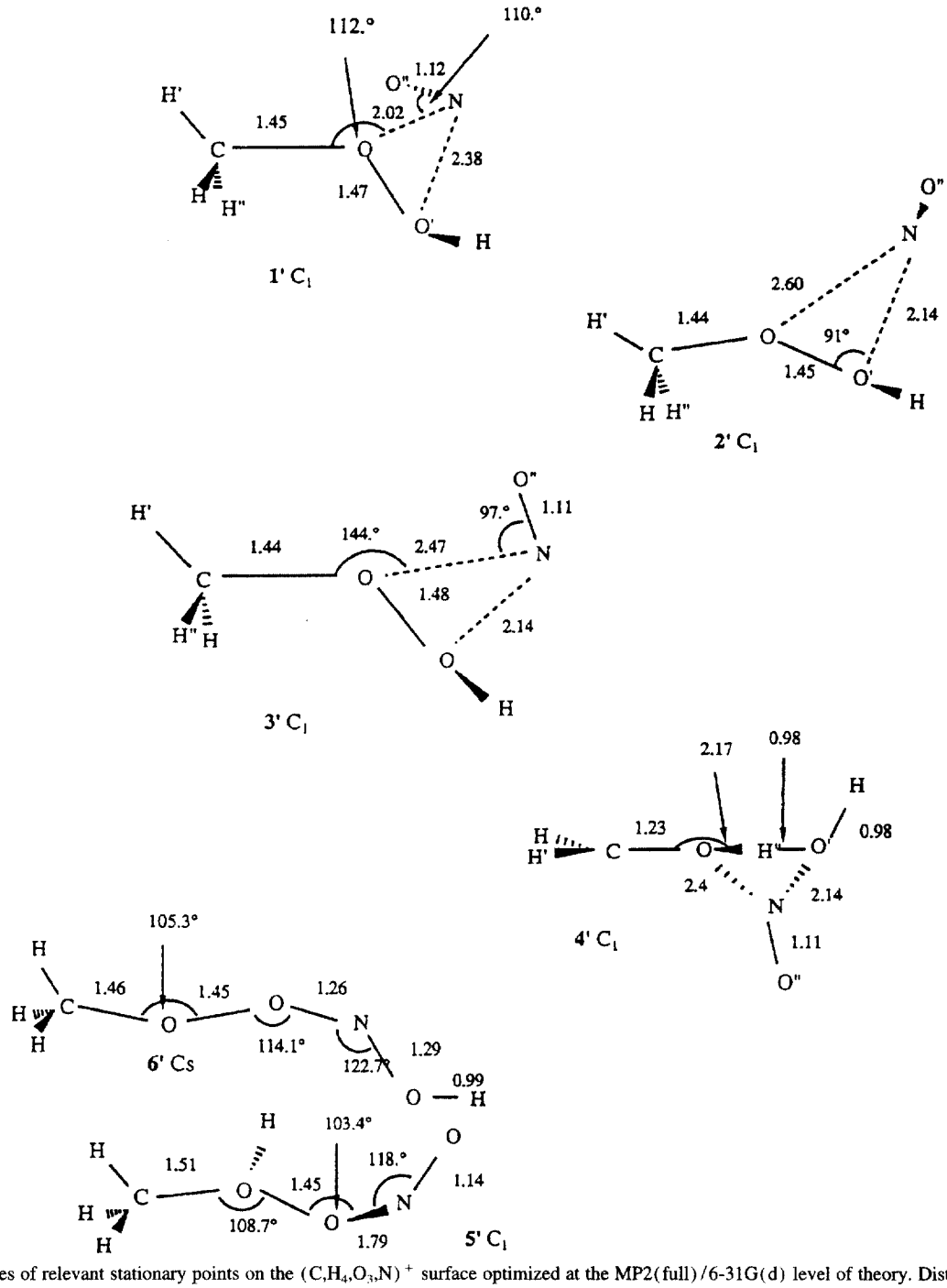

Fig. 6. Geometries of relevant stationary points on the $(C,H_4,O_3,N)^+$ surface optimized at the MP2(full)/6-31G(d) level of theory. Distances (Å), angles (°).

energies reported in Table 6 and their entropies [2], the absolute standard free energies of CH_3OOH and CH_3OO^- were calculated to be -190.60777 and -190.01653 hartree molecule^{-1} at 298 K respectively, leading to a GPA (CH_3OOH) of 365.0 ± 2 kcal mol^{-1}, practically the same value obtained from the experimental measurement.

[2] The $S°(H^+)$ was calculated from the Sackur–Tetrode equation.

5. Discussion

The theoretical and experimental results concur in outlining a coherent picture of the gas-phase reactivity of CH_3OOH toward charged electrophiles, pointing to the higher basicity/nucleophilicity of the α oxygen atom, as expected on the grounds of the larger inductive effect of CH_3 than of H. This trend holds both in the protonation and in the methylation of

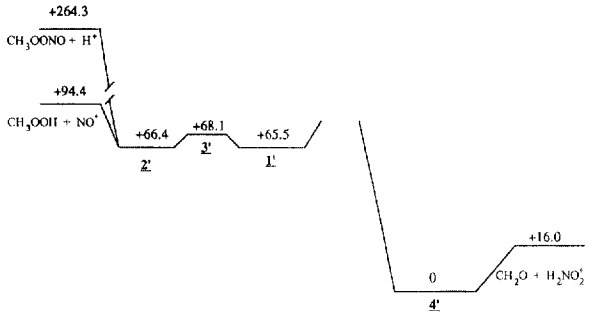

Fig. 7. Energy profile (0 K) of the relevant portion of the $(C,H_4,O_3,N)^+$ surface of the MP4(SDTQ)/6-311(d,p)//MP2(full)/6-31G(d) level of theory. Distances (Å), angles (°).

1, which yield **2** and **2″** as the most stable adducts, in accord with the theoretical results, whose reliability is supported by the excellent (perhaps to some extent fortuitous) agreement between the experimental and the calculated PA of CH_3OOH, 173.3 ± 2 versus 172.6 kcal mol^{-1}. The agreement is somewhat less satisfactory in the case of CH_3OOCH_3, whose experimental and theoretically computed PA values are 176.2 ± 4 and 180.4 ± 2 kcal mol^{-1} respectively. In this case, owing to the problems affecting the experimental measurement, related to the lack of suitable reference bases and the occurrence of side reactions, the theoretical PA value is regarded as more reliable. It is worth mentioning that the PA values of both CH_3OOH and CH_3OOCH_3 are intermediate between those of water and methanol, 165.0 and 181.7 kcal mol^{-1} respectively [22]. Passing to nitrosation of CH_3OOH, the agreement between experiment and theory is even less satisfactory, since apparently the calculations performed at the MP4(SDTQ)/6-311G(d,p)//MP2(full)/6-31G(d) level of theory overestimate the NO^+ BE of **1**, giving a value of 28.7 kcal mol^{-1}, versus an experimental value, 22.4 ± 3 kcal mol^{-1}, which is in line with the BE of comparable nucleophiles and agrees with the value 23.0 ± 2 kcal mol^{-1} obtained by introducing the experimental PA of **1** into the recently reported general correlation between the NO^+ BE and the PA of n-type nucleophiles [25].

As to the acidity of **1**, its experimental GPA of 365.1 ± 4 kcal mol^{-1}, in excellent agreement with the theoretically calculated value 365.0 ± 2 kcal mol^{-1}, characterizes CH_3OOH as an acid whose strength is close to that of H_2O_2 (GPA = 368.5 kcal mol^{-1}) and exceeds those of H_2O and CH_3OH, whose GPA values are 384.1 and 374.0 kcal mol^{-1} respectively [21].

Passing to structural aspects, the G2 potential energy diagram of Fig. 3 allows a reasonable explanation of the MIKE and CAD results, pointing to the incomplete conversion of the $(CH_3OOH)H^+$ ions from Eq. (1), A = H_2O, to the **PBD 5**. In fact, from the above reported PA data it is clear that both **2** and **3** can be formed from the reaction. However, only protomer **3** is liable to conversion into **5** via a sequence of low-barrier (≤ 10 kcal mol^{-1}) steps, whereas protomer **2** is located in a deeper well, and its conversion into **3**, and hence into **5**, requires overcoming a barrier of ~ 37 kcal mol^{-1} (Fig. 3). Given the relatively low exothermicity of their formation process, it seems likely that most ions **2** survive conversion into **5** and represent the major component of the $(CH_3OOH)H^+$ population when the latter is subjected to structural analysis after a delay of ~ 10 ms.

Table 9
Comparison of theoretically calculated and experimental thermochemical quantities at 298 K (kcal mol^{-1})

		This work		Ref. [17] Theory
		Experiment	Theory	
CH_3OOH PA	α oxygen	173.3 ± 2	172.6 ± 2	171.9
	β oxygen		168.1 ± 2	170.0
CH_3COOCH_3 PA		176.2 ± 2	180.4 ± 2	178.9

The experimental results concerning methylation of **1** find a satisfactory rationalization in the theoretical picture of the $(C_2,H_7,O_2)^+$ systems, pointing to the comparable stability of ions **2″** and **3″**, located in relatively deep wells and separated by a relatively high barrier. This accounts for the MIKE and CAD evidence pointing to the formation of a mixed **2″/3″** population from Eq. (4).

Passing to gas-phase nitrosation of **1**, the peculiar structure of the most stable adduct **4″**, described theoretically as a species capable of undergoing H^+ or NO^+ transfer to gaseous bases/nucleophiles, is consistent with the FT-ICR evidence for the occurrence of Eq. (8a) and (8b).

As a closing remark, it is most rewarding that, whenever comparable, the present results are in excellent agreement with those of a very recent mass spectrometric study on the unimolecular fragmentation of protonated methyl hydroperoxide and dimethyl peroxide, complemented by ab initio calculations at the B3LYP/6-311++G** level of theory [17]. The degree of agreement is apparent from Table 9, where the thermochemical data from the two studies are compared.

6. Supplementary material

The optimized geometrical parameters of the species of interest are available from the authors on request.

Acknowledgements

The financial support from the Universities of Rome 'La Sapienza', and 'Tor Vergata' and the CNR is gratefully acknowledged. The authors thank Professor H. Schwarz for a preprint of his paper on the cleavage of protonated methyl hydroperoxide and dimethyl peroxide. The help of F. Angelelli and G. D'Arcangelo who performed the FT-ICR and TQ measurements is gratefully acknowledged.

References

[1] P.A. Leighton, in The Photochemistry of Air Pollution, Academic Press, New York, 1961, p. 244.
[2] R.A. Cox, in M.J. Pilling and I.W.W. Smith (eds.), Modern Gas Kinetics, Blackwells, Oxford, 1987.
[3] T.J. Wallington, P. Dagaut and M.J. Kurylo, Chem. Rev., 92 (1992) 667.
[4] H. Niki, P.D. Maker, C.M. Savage and L.P. Breitenbach, J. Phys. Chem., 87 (1983) 2190.
[5] C.N. Hewitt and G.L. Kok, J. Atmos. Chem., 12 (1991) 181.
[6] P.D. Lightfoot, R.A. Cox, J.N. Crowley, M. Destriau, G.D. Hayman, M.E. Jenkin, G.K. Mootgart and F. Zabel, Atmos. Environ., 26A (1992) 1805.
[7] H. Schwarz and H.-M. Schiebel, in S. Patai (ed.), The Chemistry of Peroxides, Wiley, New York, 1983, p. 105.
[8] A.R. Burgess, D.K. Sen Sharma and M.J.D. White, Adv. Mass Spectrom., 4 (1968) 345.
[9] N.G. Adams and D. Smith, Chem. Phys. Lett., 79 (1981) 563.
[10] J. Glosik, A. Jordan, V. Skalsky and W. Lindinger, Int. J. Mass Spectrom. Ion Processes, 92 (1989) 37, and Refs. therein.
[11] W.J. Kirchner, J.M. Van Doren and M.T. Bowers, Int. J. Mass Spectrom. Ion Processes, 92 (1989) 37.
[12] C.A. Schalley, D. Schröder and H. Schwarz, Helv. Chim. Acta, 78 (1995) 1999.
[13] J. Glosik, A. Jordan, V. Skalsky and W. Lindinger, Int. J. Mass Spectrom. Ion Processes, 129 (1993) 109.
[14] C.A. Schalley, D. Schröder and H. Schwarz, Int. J. Mass Spectrom. Ion Processes, 153 (1996) 173.
[15] C.A. Schalley, R. Wesendrup, D. Schröder and H. Schwarz, Organometallics, 15 (1996) 678.
[16] J.H. van Driel, W. Heerma, J.K. Terlouw, H. Halim and H. Schwarz, Org. Mass Spectrom., 20 (1985) 665.
[17] C.A. Schalley, M. Dieterle, D. Schröder, H. Schwarz and E. Uggerud, Int. J. Mass Spectrom. Ion Processes, 163 (1997) 101.
[18] (a) F. Cacace, Acc. Chem. Res., 21 (1988) 215; (b) F. Cacace, M. Attinà, G. de Petris and M. Speranza, J. Am. Chem. Soc., 116 (1994) 6413; (c) F. Cacace and M. Speranza, Science, 265 (1994) 208; (d) F. Cacace, Pure Appl. Chem., 69 (1997) 227 and Refs. therein.
[19] D. Thölman and H.Fr. Grützmacher, J. Am. Chem. Soc., 113 (1991) 3281.
[20] C.A. Schalley, R. Wesendrup, D. Schröder, T. Weiske and H. Schwarz, J. Am. Chem. Soc., 117 (1995) 7711.
[21] S.G. Lias, J.E. Bartmess, J.F. Liebmann, F.L. Holmes, R.D. Levin and W.G. Mallard, J. Phys. Chem. Ref. Data, 17 (1988) suppl. 1.
[22] J.E. Szulejko and T.B. McMahon, J. Am. Chem. Soc., 115 (1993) 7839.
[23] T. Su and M.T. Bowers, in M.T. Bowers (ed.), Gas Phase Ion Chemistry, Vol. 1, Academic Press, New York, 1979, p. 84.
[24] R.G. Cooks, J.S. Patrick, T. Kotiaho and S. McLukey, Mass Spectrom. Rev., 13 (1994) 287 and Refs. therein.
[25] F. Cacace, G. de Petris and F. Pepi, Proc. Natl. Acad. Sci. (USA) 94 (1997) 3507.
[26] M.J. Frisch, G.W. Trucks, H.B. Schlegel, P.M.W. Gill, B.J. Johnson, M.A. Robb, J.R. Cheesman, T.A. Keith, G.A. Petersson, J.A. Montgomery, K. Raghavachari, M.A. AlLaham, V.G. Zakrzweski, J.V. Ortiz, J.B. Foresman, C.Y. Peng, J. Cioslowski, B.B. Stefanov, A. Nanayakkara, M. Challacombe, P.Y. Ayala, W. Chen, M.W. Wong, J.L. Andres, E.S. Reploge, R. Gomperts, R.L. Martin, D.J. Fox, J.S. Binkley, O.J. Defrees, J. Baker, J.P. Stewart, M. Head-Gordon, C. Gonzales and J.A. Pople, Gaussian 94 (Revision D.3), Gaussian, Pittsburgh, PA, 1995.
[27] G. Peng and H.B. Schlegel, Isr. J. Chem., 33 (1993) 449.
[28] M. Jonsson, J. Phys. Chem., 100 (1996) 6814.
[29] J. Koller, M. Hodoscek and B. Plesnicar, J. Am. Chem. Soc., 112 (1990) 2129.